

# Closed-loop control of seizure activity via real-time seizure forecasting by reservoir neuromorphic computing

Maryam Sadeghi<sup>1†</sup>, Darío Fernández Khatiboun<sup>1†</sup>, Yasser Rezaeiyan<sup>1†</sup>, Saima Rizwan<sup>2</sup>, Alessandro Barcellona<sup>3</sup>, Andrea Merello<sup>3</sup>, Marco Crepaldi<sup>3</sup>  
Gabriella Panuccio<sup>2\*</sup> and Farshad Moradi<sup>1\*</sup>

<sup>1</sup>ICELab, Department of Electrical and Computer Engineering, Aarhus University, Aarhus, 8200, Denmark.

<sup>2</sup>Enhanced Regenerative Medicine Lab, Istituto Italiano di Tecnologia, Genova, 16163, Italy

<sup>3</sup>Electronic Design Laboratory, Istituto Italiano di Tecnologia, Genova, 16152, Italy

\*Corresponding authors. E-mails:

Gabriella Panuccio: [gabriella.panuccio@iit.it](mailto:gabriella.panuccio@iit.it)

Farshad Moradi: [moradi@ece.au.dk](mailto:moradi@ece.au.dk)

†These authors contributed equally to this work.

## Abstract

Closed-loop brain stimulation holds potential as personalized treatment for drug-resistant epilepsy (DRE) but still suffers from limitations that result in highly variable efficacy. First, stimulation is typically delivered upon detection of the seizure to abort rather than prevent it; second, the stimulation parameters are established by trial and error, requiring lengthy rounds of fine-tuning, which delay steady-state therapeutic efficacy. Here, we address these limitations by leveraging the potential of neuromorphic computing. We present a system capable of driving personalized free-run stimulations based on seizure forecasting, wherein each forecast triggers an electrical pulse rather than an arbitrarily predefined fixed-frequency stimulus train. We validate the system against hippocampal spheroids coupled to 3D microelectrode array as a simplified testbed, showing that it can achieve seizure reduction >97% while primarily using instantaneous stimulation frequencies within 20 Hz, well below what typically used in clinical settings. Our work demonstrates the potential of neuromorphic systems as a next-generation neuromodulation strategy for personalized DRE treatment.

## Keywords

Neuromorphic system, drug-resistant epilepsy, seizure forecasting, neuromodulation.

## Introduction

Epilepsy is a chronic neurological disorder characterized by the persistent predisposition of the brain to generate seizures, i.e., sudden excessive electrical discharges due to hyperexcitability (1). Epilepsy affects 70 million people globally (2, 3) and carries among the highest global burden within neurological disorders (1). Between 30 to 40% of patients do not respond to anti-seizure medications (2) and are therefore diagnosed with drug-resistant epilepsy (DRE). For the latter, the current first-line treatment is the surgical resection of the epileptic focus; however, this is a no-return option that is only feasible in a subset of patients and cannot guarantee complete freedom from seizures.

Brain stimulation emerges as a valid alternative to treat DRE, as it is safe and reversible (4, 5). However, the stimulation protocols still rely on arbitrary choices made by trial and error among a nearly infinite combination of stimulation parameters (6, 7). As a result, currently achievable therapeutic outcomes are promising (8, 9), but there is still room for improvement.

Closed-loop systems, which operate based on feedback from ongoing brain activity, are at the forefront of personalized brain stimulation for DRE treatment as they are designed to deliver electrotherapy when it's most needed. The Responsive Neuro Stimulation (RNS) system is the emblem of such closed-loop devices, and it is currently the only one approved by the Food and Drug Administration. The RNS (and similarly other closed-loop devices still in preclinical research) is primarily designed to respond to the detection of a seizure so to abort it at its onset (10). However, this approach is sub-optimal for two interrelated reasons: (i) ideally, the seizure should be prevented rather than aborted and (ii) once the seizure has started, it might be difficult to entrain the epileptogenic network. Particularly, cases of sudden unexpected death in epilepsy can still happen (11) although at a reduced incidence (3).

Seizure prediction has long been considered the method of choice to provide preventive stimulation therapy. However, it is a deterministic approach in that it aims at predicting the seizure onset within an arbitrarily defined time window (i.e., the prediction horizon). As such, it disregards that seizure generation is a dynamical process that does not follow a linear time course; thus, stimulation within a fixed time window before the seizure may yield opposite effects depending on the dynamical state of the epileptogenic network at the time of stimulation (12). Seizure forecasting, a probabilistic approach that continuously assesses the likelihood of seizure occurrence (13), is emerging as a better approach to inform the optimal stimulation timing throughout the interictal-to-ictal continuum. Still, the lack of well-defined electrographic biomarkers to obtain such likelihood estimation in real time prevents leveraging the full potential of seizure forecasting for personalized preventive stimulation. Machine learning-based

approaches promise to overcome this limitation (13, 14, 15), but they come at the cost of power- and computation-hungry devices. In this framework, neuromorphic ('brain-inspired') systems are gaining momentum for their potential in low-power computation-efficient biomedical applications, including signal processing and neuromodulation, thanks to their appealing potential to replicate the energy-efficient functionality of the human brain and emulate the information processing of biological neurons (16). Particularly, neuromorphic systems permit encoding information using spike trains (17), thus enabling event-driven computation. Moreover, the spatiotemporal sparsity of their neural activity supports implementing highly energy-efficient systems (18).

Building on this concept, we have designed and implemented a neuromorphic computing system (NCS) on FPGA leveraging reservoir computing and trained it for real-time seizure forecasting supporting closed-loop electrical stimulation to prevent seizures. Using rodent hippocampal spheroids as a simplified in vitro testbed, we demonstrate that the NCS can reduce seizure activity by >97% while delivering ad-hoc patterned stimulation, operating most of the time in the low-frequency stimulation range. Our work paves the way for a new generation of power- and computation-efficient neuromodulation devices grounded on seizure forecasting to treat DRE.

## **Materials and Methods**

### **Hippocampal Spheroids Preparation and Maintenance.**

Hippocampal spheroids were prepared from Sprague-Dawley rat embryonic hippocampi harvested at embryonic age E17.5 and processed as detailed in (19). For each spheroid, 30,000 cells were seeded in each well of an ultra-low adhesive U-shaped 96-well plate (Cell Carrier™ -96, PerkinElmer) with 200  $\mu$ l of Neurobasal medium supplemented with 2% B27, 1% PenStrep and 1% Glutamax. On the third day after seeding, the spheroids were transferred to a 24-well plate coated with 3% agarose (UV-treated for 15-20 min), one spheroid per well. Neurobasal medium was replaced weekly by 50%. Spheroids were maintained in a cell culture incubator at 37°C and 5% CO<sub>2</sub>. Reagents were purchased from Thermo Fisher, Italy.

### **Microelectrode Array Electrophysiology**

Extracellular field potential recordings were performed acutely via 3D MEA (8x8 layout, TiN electrodes, diameter 12  $\mu$ m, height 80  $\mu$ m, inter-electrode distance 200  $\mu$ m, impedance  $\sim$ 150 k $\Omega$ , internal reference electrode) using the MEA2100-mini-HS60 amplifier connected to the IFB v3.0 multiboot interface board through the SCU signal collector unit. Signals were sampled at 5 kHz (lowpass filtered at 2 kHz before

digitization), acquired via the Multichannel Experimenter software and stored in the PC hard drive for offline analysis. All recordings were performed in artificial cerebrospinal fluid (ACSF) composed of (mM): NaCl 117, KCl 3.75,  $\text{KH}_2\text{PO}_4$ , 1.25,  $\text{MgSO}_4$  0.5,  $\text{CaCl}_2$  2.5, D-glucose 25,  $\text{NaHCO}_3$  26, L-Ascorbic Acid 1. The ACSF was maintained at  $\sim 37^\circ\text{C}$  with the use of a custom-made heating lid covering the headstage, along with the warming of the MEA amplifier base, and equilibrated at pH  $\sim 7.4$  through humidified carbogen delivered via a tubing connected to the heating lid. The recording temperature was controlled by a TC02 thermostat and checked with a k-type thermocouple in all experiments.

Each spheroid was taken from the cell culture incubator immediately before the experimental session and placed onto the 3D MEA, where it was let habituate for 20-30 minutes until steady-state activity before recording. The equipment for MEA electrophysiology and temperature control was purchased from Multichannel Systems (MCS), Reutlingen, Germany. Chemicals for the ACSF were purchased from Sigma-Aldrich, Italy.

### ***NCS Hardware Description, Operation, and Implementation***

The NCS monitors and processes the spheroid's electrical activity in real-time to trigger the activation of the stimulator according to the resulting forecasts. The system operates synchronously to a system clock of frequency  $f_{sysclk}$ , processing the input signals at an input sampling frequency  $f_{in}$ . At each  $f_{in}$  clock cycle, the NCS updates the membrane potentials of all neurons in each layer by sequentially iterating over all the respective pre-synaptic neurons associated with the neuron being updated. The updates are governed by the accumulation of synaptic weights associated with the firing activity of pre-synaptic neurons at the time of the processing. This architecture employs time-division multiplexing, allowing a single neuromorphic processing unit (NPU) to sequentially handle the processing of all neurons within the layer. By sharing the NPU circuit across the network we reduce the total number of resources, and the leakage power derived from them. The neuron models use 12-bit and 16-bit fixed-point representation to model their membrane potential (for reservoir and readout layer, respectively) and an 8-bit leakage constant factor configurable to model multiple dynamics of the neuron behavior. Similarly, the synaptic connections and weights use 8-bit and 12-bit, respectively, for reservoir and readout layer. All synaptic connections and neuron membrane potentials are stored in static random-access memories (SRAMs). Synaptic connections require two SRAMs of 64 KB and 6 KB, while membrane potentials require two SRAMs of 0.375 KB and 0.125 KB (for both reservoir and readout layer respectively). Additionally, the NCS implements an online training algorithm, R-STDP, enabling real-time updates of synaptic weights to better adapt its synaptic connectivity based on the ongoing spheroid activity. The R-STDP model,

represented in equation 1, operates based on principles of the STDP learning process. While STDP is traditionally considered as an unsupervised algorithm, R-STDP incorporates the influence of a neuromodulator to regulate the weight updates. These updates are ruled by a label signal,  $label(t)$ , to combine both STDP and anti-STDP long term potentiation/depression (LTP/LTD) processes during the training phase:

$$\Delta w_{STDP} \begin{cases} \Delta w^+ = A_+ \cdot e^{\left(\frac{-|\Delta t|}{\tau_+}\right)} \text{ if } \Delta t > 0 \\ \Delta w^- = A_- \cdot e^{\left(\frac{-|\Delta t|}{\tau_-}\right)} \text{ if } \Delta t < 0 \end{cases} \quad (1)$$

$$\Delta w_{antiSTDP} \begin{cases} \Delta w^+ = -A_+ \cdot e^{\left(\frac{-|\Delta t|}{\tau_+}\right)} \text{ if } \Delta t > 0 \\ \Delta w^- = -A_- \cdot e^{\left(\frac{-|\Delta t|}{\tau_-}\right)} \text{ if } \Delta t < 0 \end{cases}$$

Where  $A_{\pm}$  refers to the amplitude of the weight update,  $\Delta t$  refers to the timing between postsynaptic and presynaptic spikes, and  $\tau_{\pm}$  is the time constant of the learning curve. The NCS stores a sampled version of both  $\Delta W_{STDP}$  and  $\Delta W_{antiSTDP}$  in a look-up table (LUT), thereby reducing the computational complexity associated to the weight update. Furthermore, this LUT-based approach enables flexibility in varying learning parameters and curve shapes, supporting a range of applications. The LUT stores two 64 values of 8-bit signed fixed precision (64 values for each LTP/LTD) processes in a series of SRAMs of 0.125 KB.

The hardware model of the NCS is also developed using Python 3.9.0 in conjunction with NEST Simulator v3.6.0 and its modeling language NESTML. This approach ensures that the models of both neuron and learning algorithms meet the constraints imposed by digital circuitry. Finally, hardware simulations were conducted using Xilinx Vivado 2022.2 and implemented on a Zybo Z7 SoC FPGA development board. The NCS implemented in the FPGA initializes the synaptic weights from both reservoir and readout layer using the weights obtained during training.

### Software simulations

To test and optimize the NCS before physical deployment, we simulated its behavior using a co-simulation environment with the NEST simulator framework in Python 3.12, allowing precise replication of the hardware functionality.

As described in (19), the epileptiform phenotype of these spheroids may be purely interictal (i.e., no ictal activity), or comprise both interictal and ictal events. This behavior suggests that the information conveyed by interictal events carries different values for seizure forecasting. Thus, distinguishing these events may support the design of robust seizure forecasting systems. To this end, we trained a first neuron

to become sensitive to interictal discharges coexisting with ictal activity, and a second neuron to respond to interictal discharges appearing in isolation (i.e., in spheroids not generating ictal activity). The dataset used is a subset of what is described in (19), consisting of six 20-minute MEA recordings from hippocampal spheroids, originally digitized at 20 kHz and resampled for this work at  $f_{in} = 2$  kHz. The dataset organizes the recorded discharges into labeled 50-second segments based on their recordings, combining them into a single time series. Ictal discharges are then removed from the recordings, dissipating their temporal relation with the interictal events and, at the same time, the interictal time series itself, to enhance the robustness of the training process. In summary, the dataset combines both baseline and interictal activity from both types of electrical phenotypes generated by the spheroids, with each interictal segment labeled accordingly (i.e., ‘seizure’ and ‘no seizure’). In addition, we included a transition period with no activity of 1 second duration to separate the recording segments. This transition allows the SNN to reach an equilibrium state before processing the next recording segment, avoiding cumulative processing biases.

During the training process, the NCS processes each sample in an online fashion, updating the synaptic weights dynamically based on STDP relationships. The training phase consisted of 50 epochs, with weight adjustments occurring at each timestep to reinforce neuronal activity. To evaluate the model’s performance, we used a separate testing set composed of segments from two spheroids to ensure no overlap with training data.

The final NCS configuration is composed of 2 input channels (from the SFE algorithm), 128 reservoir neurons (118 excitatory neurons and 10 inhibitory neurons) from which 64 neurons are connected to 2 readout neurons in a feedforward layer. The connectivity between the reservoir neurons is randomly generated and their synaptic weights are randomly initialized by a normal distribution with mean  $\mu=64$  and standard deviation  $\sigma=12$ .

### **Closed-loop electrical stimulation driven by the NCS**

Square biphasic current pulses (100  $\mu\text{s}$ /phase, positive phase first) were delivered in monopolar configuration through a selected MEA electrode. We chose the current intensity based on a ‘fast’ input/output (I/O) curve starting at 150  $\mu\text{A}$ , aimed at finding the stimulus intensity that would reliably ( $\geq 80\%$  probability) evoke an interictal-like response (31) without triggering after discharges (i.e., population bursts  $> 2$  s (32)).

The bidirectional communication between the NCS and the spheroid coupled to the MEA system relied on a custom interface PCB reading the MEA signals from the MCS SCU analog output via the SCU 68-

pin analog output connector and feeding them to the NCS; a custom graphical user interface enabled selecting the feedback electrode. The NCS forecasts were then sent as TTL pulses (0-3.3 V) back to the custom interface PCB through which they were sent to the selected digital input of the MCS IFB v3.0 via its dedicated digital I/O 68-pin connector. The TTL pulses were then detected by the Digital Event Detector via the Multichannel Experimenter software, in turn activating the built-in stimulator of the MEA system. For each spheroid, we selected the feedback electrode from those showing electrical activity based on the signal-to-noise ratio, and we chose the stimulation electrode from those surrounding the feedback electrode based on the reliability and propagation of evoked responses during the fast I/O step.

Pre- and post-stimulus recordings were pursued for at least 20 minutes to ensure that the final recording segment (from the onset of the first to the end of the last recorded ictal event) was aligned with the 20 min duration of the NCS-driven stimulation session for a robust comparison of the %time in ictal state across the experimental phases. We chose a stimulation session duration of 20 minutes based on the average interval between ictal discharges, so to be  $\geq 3$  times the interval observed during pre-stimulus baseline, coherent with the guidelines of the International League Against Epilepsy on the definition of seizure freedom (33).

The NCS was tuned manually during the pre-stimulus baseline recording, starting from a list of available parameters established empirically during the testing phase of the NCS against pre-recorded MEA signals. The NCS behavior had to meet the following specifications: (i) it would respond primarily during the signal noise floor (forecasting) rather than to the epileptiform events (detection); (ii) it would never respond solely to ictal activity (seizure detection); (iii) if an ictal discharge or an afterdischarge would occur, it would not stimulate during their initial (tonic) phase since the biological network is in a non-permissive state and would not be possible to entrain it via electrical stimulation.

### **Data and Statistical Analysis**

Epileptiform discharges were labeled by expert neurophysiologists using a semi-automated approach based on an automated event detection algorithm followed by inspection and manual correction of the obtained labels, as required. The software for event labeling, running in a graphical user interface, was written in MATLAB R2021b (MathWorks, Natick, USA).

To evaluate the degree of ictal activity reduction, we computed the % time spent by the spheroids in the ictal state, as described in (29). We adopted this approach instead of measuring the duration and inter-event interval of the ictal discharges to account for the possibility of only observing one or two ictal events during electrical stimulation, which would bias the quantification of the degree of ictal activity

reduction.

For statistical comparison of the %time spent in the ictal state, we first checked the dataset for normality (Shapiro-Wilk test) and homoscedasticity (Levene test). Since the dataset was neither normally distributed ( $p = 0.002$ ) nor homoscedastic ( $p = 0.02$ ), we used one-way ANOVA followed by the non-parametric Games-Howell post-hoc test for multiple comparisons. We considered differences to be statistically significant if  $p < 0.05$ . To compute the statistical power achieved, we performed a posteriori analysis using the freely available software G\*Power. Throughout the text, data are expressed as mean  $\pm$  SD, unless otherwise specified.

## Results

### Closed-loop operation of the neuromorphic computing system

**Figure 1** illustrates the closed-loop architecture for electrical stimulation driven by seizure forecasting operated by the NCS (see Methods for full details). The architecture comprises commercial microelectrode array (MEA) electrophysiology equipment, interfaced with the FPGA-implemented NCS via a custom interface PCB. As a simplified biological testbed, we used rodent primary hippocampal spheroids, which spontaneously generate epileptiform activity consisting of ictal (seizure) and interictal (between seizures) events (19). Signals are recorded from a spheroid coupled to a 3D MEA and subsequently amplified using an adjustable multi-channel analog front-end to enhance signal quality for further processing. The amplified signals are then digitized via 12-bit FPGA's ADCs, sampled at 4 kHz, and fed into an encoder. The encoder converts input signals into spikes based on signal dynamics, generating two spike streams. These are processed by the NCS which comprises two layers. The first layer is a reservoir network consisting of leaky integrate-and-fire (LIF) neurons. This layer connects a network of excitatory and inhibitory neurons (256 neurons in total) using fixed, randomly assigned synaptic weights. These connections create recurrent pathways, enabling the reservoir to perform complex nonlinear transformations and map the input data into a high-dimensional output space while extracting temporal features in real-time. The output of this reservoir layer comprises the activity of 64 out of the 256 neurons. The second layer is a trainable readout layer consisting of 2 LIF neurons, which receive the output of the reservoir. This readout layer employs a reward-modulated spike-timing-dependent plasticity (R-STDP) algorithm (20), a supervised learning approach that enables real-time training for seizure forecasting. Finally, a decision-making block interprets the readout layer's firing activity to determine whether to activate the built-in stimulator of the MEA system (see Methods). This yields an ad-hoc stimulation pattern mirroring the timings of the true states in the decision-making block,

i.e., each true state triggers a single electrical pulse instead of activating a stimulus train of predefined frequency and duration.

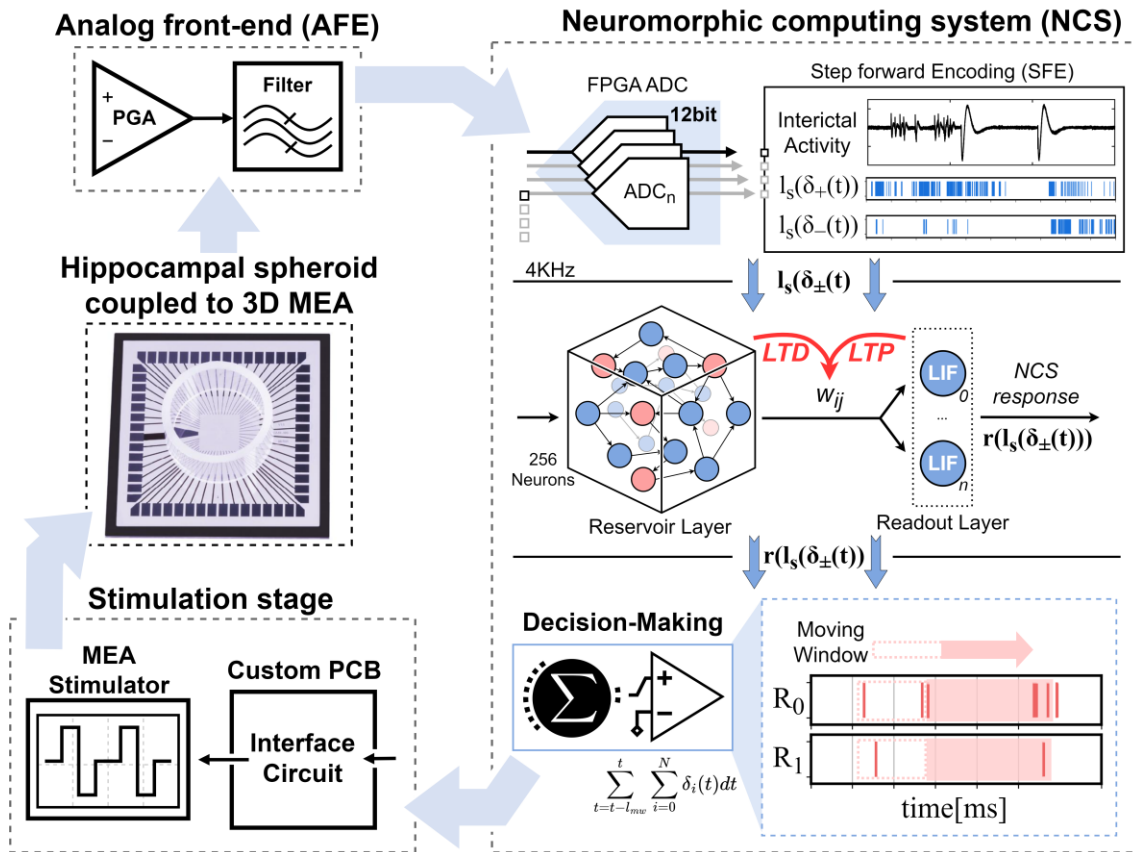


**Figure 1. Closed-loop operation of the neuromorphic computing system.**

Signals recorded from a rodent hippocampal spheroid using a 3D MEA are amplified by the analog front-end (AFE), producing a voltage signal in the range of 0 to 1 V. The signal is then digitized by the ADC and converted into spike streams by the encoder. The spike data is processed through reservoir and readout layers, and the decision-making block forecasts seizures. Positive forecasts then trigger stimulation to prevent seizure activity.

### **Epileptiform signals capturing and spike encoding by the neuromorphic computing system**

**Figure 2A** shows a simplified schematic of the analog front-end (AFE), which consists of a differential readout channel, a blanking circuit, a closed loop driven right leg (DRL) circuit, and a digital offset cancellation loop. At the input stage, two buffers increase the input impedance of the front-end and enhance its common-mode rejection ratio (CMRR). The buffered signals are fed into an AC-coupled instrumentation amplifier (IA) to remove the electrodes' offset and avoid the amplifier's saturation. Furthermore, a ground-isolated balanced AC-coupling circuit improves the CMRR and eliminates direct signal paths from the IA input to the grounds. This circuit ensures AC coupling for the differential signal while providing a biasing path for the IA. The gain of the IA is adjustable between 20dB-60dB using the

$R_G$  resistor. Following the IA, a fourth-order Butterworth low-pass filter is employed, offering a bandwidth of 10 kHz which enables the sensing of both action potential and local field potentials. This filter achieves  $>75$  dB attenuation in the stopband at 100 kHz and maintains passband ripple below 1 dB, ensuring high signal fidelity.

The AFE is biased such that the output common-mode voltage is set to half the ADC's full-scale range, optimizing the output swing. However, the IA's offset variations can shift the output common-mode voltage at high gain settings. To mitigate this, the digital offset cancellation loop stabilizes the output common-mode voltage at 0.5 V, corresponding to the midpoint of the ADC's range. At the start of channel activation, the input channel is temporarily shorted to ground, and the output voltage is monitored by the FPGA's ADC. If the common-mode voltage deviates from 0.5 V, the DAC output is adjusted to realign the output common-mode voltage to the desired 0.5 V level. This ensures reliable operation and prevents offset-induced distortions.

The blanking circuit temporally grounds the input of the readout channel during electrical stimulation since the input signal amplitude may exceed the dynamic range of the readout channel due to the stimulation artifact. The latter may indeed lead to signal saturation, which, in turn, may result in the loss of critical data during the recovery time of the saturated channel. The blanking circuit thus eliminates the risk of saturation, ensuring consistent and stable operation of the system.

**Figure 2B** illustrates the encoding algorithm. This uses three combined parameters consisting of threshold-crossing and the step-forward encoding (SFE) method (21). The latter uses two SFEs with thresholds  $\theta_{low}$  or  $\theta_{high}$ . Each SFE generates a spike stream whenever the absolute value of the signal changes by more than its respective threshold. These spike trains constitute the input signals of the reservoir through separate low and high channels. At any given time, only one channel is activated depending on whether the signal value exceeds the comparison threshold  $\theta_{comp}$ .

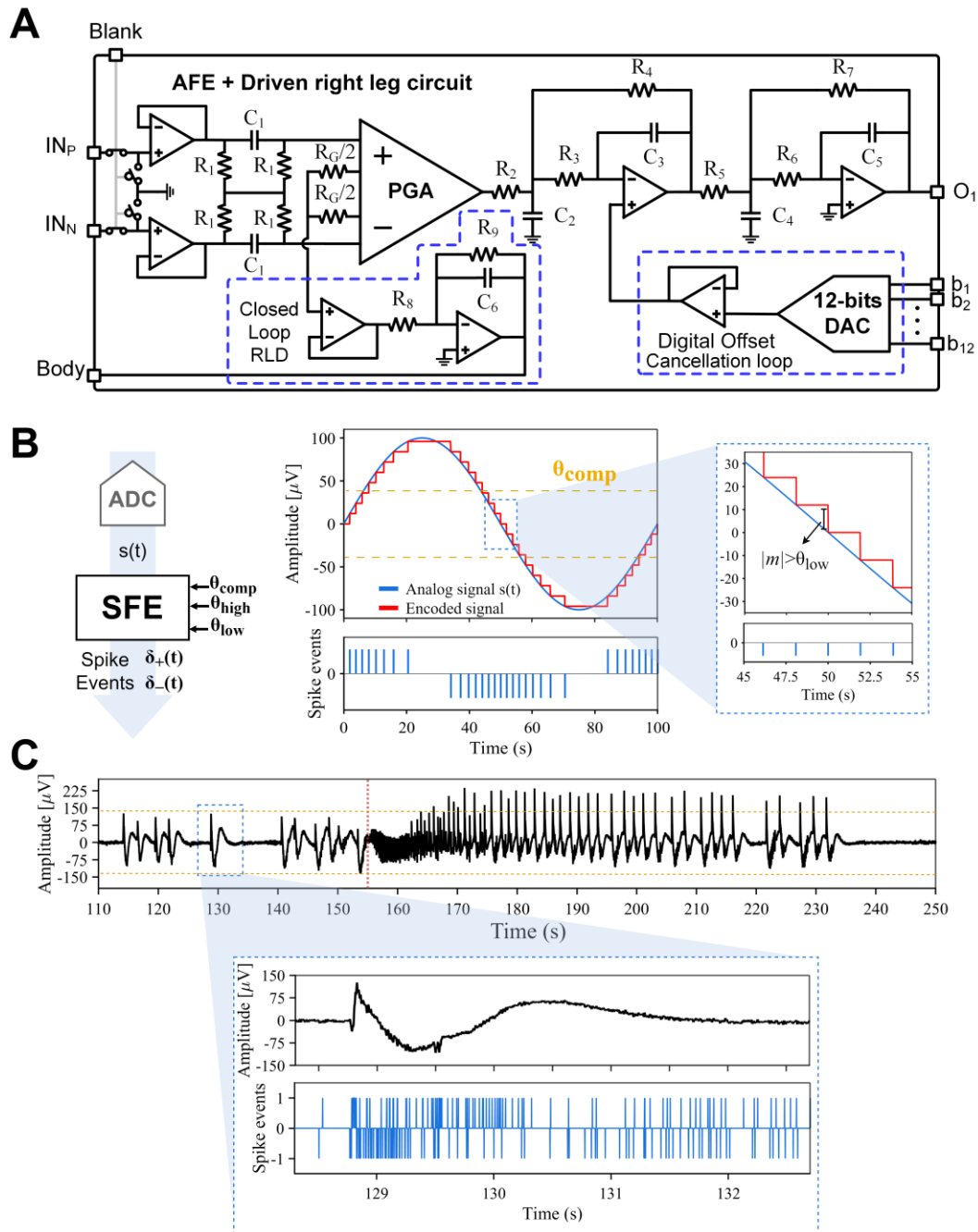


**Figure 2. Front-end architecture and spike encoding scheme.**

(A) Front-end architecture. (B) Step-forward encoding (SFE) algorithm encodes a sampled signal into spike trains, incorporating three different thresholds:  $\theta_{comp}$  to divide the signal based on its amplitude, and both  $\theta_{high}$  and  $\theta_{low}$  used in the SFE algorithm generate spikes based on the slope of the signal. (C). Example of SFE functionality applied to interictal discharges leading to seizure (onset marked by the red bar). The insert shows the SFE output in response to the interictal event framed by the blue square, consisting of a series of positive/negative spikes, the polarity of which depends on the slope sign of the interictal signal at each computation step-window.

**Figure 2C** illustrates a representative epileptiform pattern recorded from a hippocampal spheroid, including interictal events and an ictal discharge. The former are recurring short ( $\leq 2$  s-long) electrographic transients as the one framed by the dashed blue box; ictal activity (onset marked by the vertical red dashed line) is a robust ( $>10$  s-long) discharge, of slower recurring rate than interictal events, and consisting of a high-frequency oscillatory pattern (tonic phase) followed by slow-down of network activity (clonic phase) resulting in population bursts recurring at progressively longer intervals until seizure termination. In this case, the ictal discharge is heralded by a barrage of interictal events, which may thus be defined as pre-ictal activity. Interictal and ictal events are separated by epochs of baseline activity, i.e., the signal noise floor devoid of electrographic epileptiform events.

To mitigate the risk of high-amplitude interictal discharges generating a disproportionately high spike rate relative to baseline activity, the NCS spike streams are separated according to the comparison threshold to apply a higher SFE threshold for high-amplitude signals. This approach prevents bias in the training algorithm and ensures that the critical influence of baseline activity is preserved, maintaining high accuracy and robustness.

### **On-line validation of the NCS-driven stimulation in hippocampal spheroids coupled to MEA**

To validate the NCS ability to operate closed-loop control of seizure activity, we used the same hardware architecture depicted in **Figure 1**, this time enabling the control of the built-in MEA system stimulator via TTL signals generated by the NCS upon positive seizure forecasts. **Figure 3A** illustrates the experimental design for this set of experiments. **Figure 3B** shows a hippocampal spheroid coupled to a 3D MEA and the selected feedback and stimulating electrodes for the representative experiment illustrated in **Figure 3C**. The latter demonstrates the ability of the NCS to effectively drive electrical stimulation to prevent ictal activity. Upon stimulus withdrawal, seizure activity emerged back although the overall electrical pattern of the spheroid appeared to have slightly changed, suggesting a possible neuromodulation effect of the NCS-driven stimulation. The insets on the right in **Figure 3C** show the signal segments highlighted in the recording overview, at an expanded time scale, to emphasize ictal events recorded pre- and post-stimulation as well as the patterned stimulation driven by the NCS.

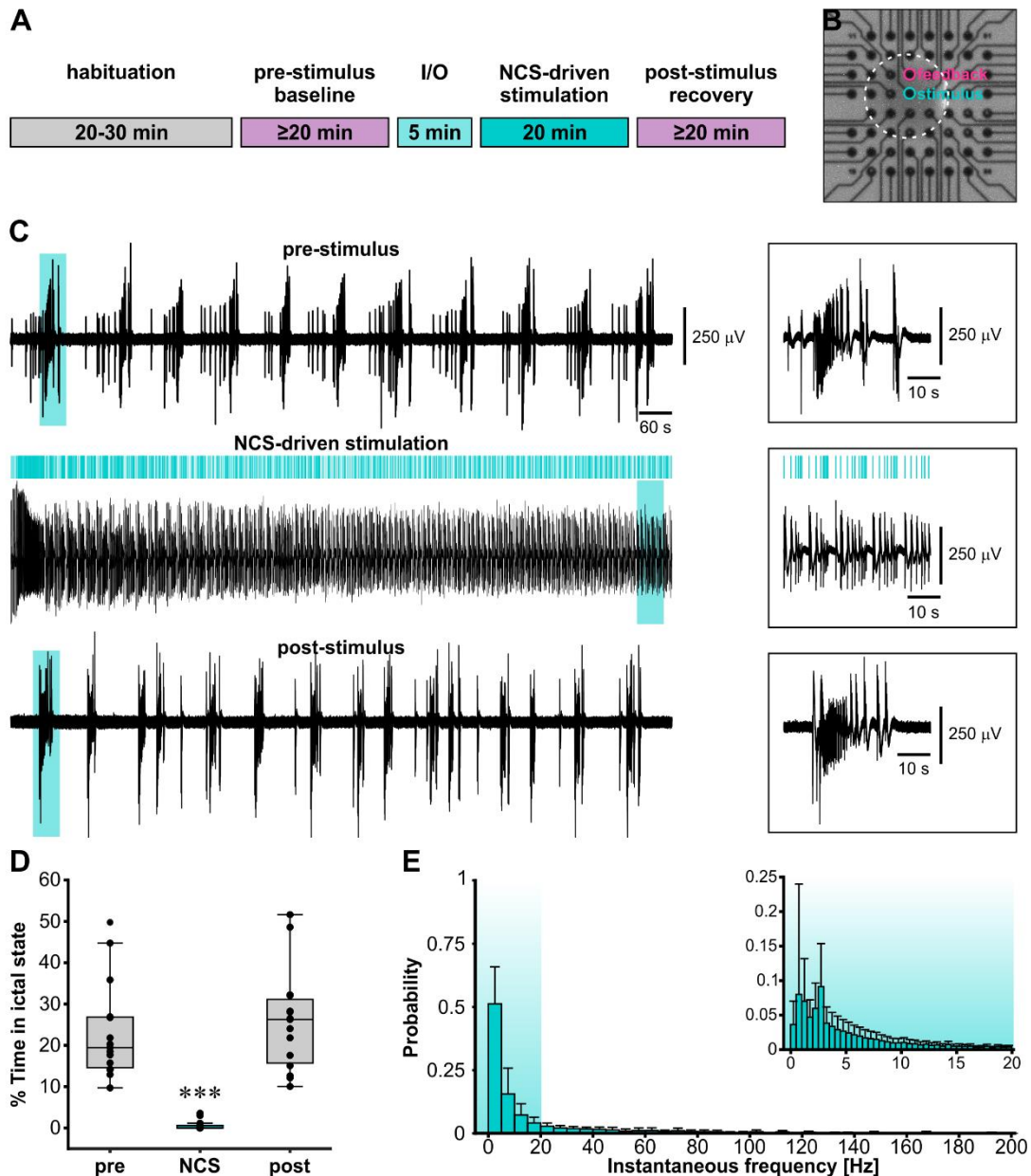


**Figure 3. Seizure activity reduction by NCS-driven patterned stimulation.**

(A) Phases of the experimental protocol. (B) Optical image of a hippocampal spheroid (outlined by the dashed white circle) coupled to a 3D MEA. (C) Representative experiment using the spheroid in (A) showing the typical pattern of recurring interictal and ictal events generated by the spheroid during pre-stimulus baseline. NCS-driven stimulation completely prevented ictal discharge generation (pulse timings are indicated by the vertical turquoise bars). Upon stimulus withdrawal, the spheroid started generating ictal discharges again. While the overall % time in ictal state (19.5%) was similar to what measured during pre-stimulus baseline (24.5%), the overall spheroid electrical pattern appeared slightly modified. The inserts on the right of each experimental phase show the signal segments corresponding to the turquoise shaded areas, visualized at a faster time scale. Note the patterned stimuli delivered by the NCS, evoking short population responses resembling interictal events. (D) Quantification and results statistics for the entire dataset (n = 15 experiments) demonstrates a statistically significant reduction of the % time in ictal state by the NCS-driven stimulation (\*\*\*) (E) Probability distributions

of the instantaneous frequency of stimulations delivered by the NCS, averaged across the experimental dataset (bin size = 5 Hz): the NCS primarily operates at instantaneous frequencies  $\leq 20$  Hz. The insert shows the probability distribution of instantaneous frequencies within 20 Hz for bin size = 0.5 Hz to further emphasize the predominance of low-frequency stimulation. Data are expressed as mean  $\pm$  SD. In the box plots, each dot represents the % time in ictal state for each experiment.

Overall, we have collected  $n = 15$  validation experiments, consistently demonstrating the dramatic reduction of ictal discharges by the NCS-driven stimulation (**Figure 3D**; %time spent in ictal state – pre-stimulus:  $23.23 \pm 11.77\%$ ; NCS-driven stimulation:  $0.59 \pm 1.15\%$ ; post-stimulus:  $25.8 \pm 12.22\%$ ; one-way ANOVA,  $F(df): 22.43(2)$ ,  $p < 0.0001$ ; Games-Howell post-hoc test:  $p < 0.0001$  stimulation vs pre- and post-stimulation,  $p = 0.99$  pre- vs post-stimulation; effect size: 0.96; power: 0.99). Analysis of the pulse timings yielded a wide range of instantaneous frequencies (0.02-714.3 Hz) consistent with the adaptive behavior of the NCS, but, remarkably, it unveiled that the system primarily operated in the low-frequency regime (**Figure 3E**): instantaneous frequencies within 20 Hz occurred with  $\sim 80\%$  probability with a large portion of the pulses ( $\sim 73\%$ ) delivered at 10 Hz or less, whereas peak frequencies  $\geq 100$  Hz were sporadic ( $\sim 3.4\%$ ).

## Discussion

We have demonstrated the potential of a reservoir NCS implementing R-STDP to perform real-time seizure forecasting driving electrical stimulation to prevent seizure activity. To this purpose, we have leveraged a high-yield in vitro model of spontaneous hippocampal epileptogenesis (19), which is relevant for addressing the most common DRE, i.e., mesial temporal lobe epilepsy. The NCS efficacy relies on its ability to robustly capture and decode distinctive features of local field potentials to forecast seizure activity through a computation- and power-efficient algorithm. Remarkably, NCS-driven stimulation achieved an outstanding reduction in seizure activity ( $>97\%$ , i.e., approximating seizure prevention) while primarily using instantaneous stimulation frequencies within the low frequency range. These features denote the potential of the NCS as a neuromodulation device supporting longer battery life, reduced electrode deterioration and brain tissue stress compared to current closed-loop devices relying on computationally demanding algorithms and typically operating in high stimulation frequency ranges (23, 24).

It is worth noting that while high-frequency stimulation is typically preferred in clinical practice, low-frequency stimulation protocols are still much studied in a continued effort to improve both the therapeutic efficacy and the battery life of the neurostimulation device. Particularly, on-demand low-

frequency stimulation has demonstrated a valid approach both in preclinical (25) and clinical (24) most recent studies. The schismatic debate around the benefit of high- versus low-frequency stimulation reflects one major outstanding challenge in neuromodulation, i.e., finding the most effective stimulation parameters (7). In this regard, comparative clinical studies, such as (26), emphasize the importance of tailoring the stimulation to the patient's needs. Still, the current approach to devising personalized neurostimulation therapies relies on on-demand open-loop stimulation using arbitrarily predefined stimulation frequencies, the quest of which is still based on trial-and-error practices. In addition, clinically approved closed-loop devices are designed to deliver stimulation upon detection of a seizure (e.g., (27)) or of signal features that, when combined, encode high likelihoods of transition to seizure (28). These approaches only partially meet the definition of personalized adaptive treatment and we argue that they lend themselves to sub-optimal efficacy. When stimulation is delivered upon seizure detection, the aim of the therapy is terminating rather than preventing the seizure; thus, the patient might still experience clinical symptoms; moreover, the epileptogenic network might not respond to stimulation (11). On the other hand, when stimulation is delivered during high likelihood of transitioning to seizure, it might trigger a seizure beforehand (30). In keeping with these concepts, a recent study has found it more beneficial stimulating during low likelihood of transition to seizure (15).

The NCS presented here operates in a radically new way by using free-run stimulations that are not constrained by pre-defined stimulus trains. This operating mode inherently supports truly personalized neuromodulation therapies as the output forecasts of the NCS are directly translated into electrical stimulation. To our best knowledge, this is the first demonstration of such a neuromodulation system.

## **Conclusion**

Although our work relies on a simplified in vitro testbed, it fosters a new mindset in the neuromodulation field by demonstrating the potential of ad-hoc free-run stimulation to prevent seizure occurrence. One limitation of the NCS is the need to manually tune its major operating parameters by a knowledgeable person. While this task is negligible compared to the current trial-and-error approach to searching for the optimal stimulation strategy, it is still a rather time-consuming step. Future directions to bolster the full potential of the NCS will be validating its efficacy in epileptic animals and equipping it with a machine-learning algorithm for auto-tuning its operating parameters.

## **Acknowledgments**

The authors thank Marina Nanni, Alice De Benedetti and Andrea Arena for their technical support for the spheroid cultures; Dr. Giacomo Pruzzo for technical support with the electrophysiology equipment and for having designed and made the custom heating lid for MEA electrophysiology.

## **Ethical statement**

The procedures involving animals were approved by the animal welfare board of Istituto Italiano di Tecnologia and by the Italian Ministry of Health (refs. 176AA.N.9AU and 176AA.N.UWY).

## **Funding**

This work has been supported financially by the European Union Horizon 2020, FET Proactive (RIA)-2018, HERMES – Hybrid Enhanced Regenerative Medicine Systems, Grant Agreement n. 824164, and by Innovations-Fonden under PIPESENSE project (0224-00056B)

## **Author contributions**

Conceptualization: MS, GP, FM.

Methodology: MS, DFK, GP, FM

Software/Hardware: DFK, YR, AB, AM, MC, GP

Validation: MS, DFK, YR, SR, GP

Formal analysis: MS, GP

Investigation: SR, GP

Resources: MC, GP, FM

Data Curation: GP

Writing - Original Draft: MS, DFK, YR, SR, GP, FM

Writing - Review & Editing: All

Visualization: MS, DFK, YR, GP

Supervision, project administration, funding acquisition: GP, FM

## **Data and materials availability**

All data, code, and materials will be shared upon reasonable requests from qualified researchers with respect to intellectual property protection.

## **Conflict of interest statement**

None of the authors has any conflict of interest to declare.

## References

1. C. Begley, R. G. Wagner, A. Abraham, E. Beghi, C. Newton, C. S. Kwon, D. Labiner, A. S. Winkler, The global cost of epilepsy: A systematic review and extrapolation. *Epilepsia* **63**, 892–903 (2022).
2. W. Löscher, H. Potschka, S. M. Sisodiya, A. Vezzani, Drug resistance in epilepsy: Clinical impact, potential mechanisms, and new innovative treatment options. *Pharmacol. Rev.* **72**, 606–638 (2020).
3. O. Devinsky, D. Friedman, R. B. Duckrow, N. B. Fountain, R. P. Gwinn, J. W. Leiphart, A. M. Murro, P. C. Van Ness, Sudden unexpected death in epilepsy in patients treated with brain-responsive neurostimulation. *Epilepsia* **59**, 555–561 (2018).
4. S. Ghosh, J. K. Sinha, S. Ghosh, H. Sharma, R. Bhaskar, K. B. Narayanan, A comprehensive review of emerging trends and innovative therapies in epilepsy management. *Brain Sci.* **13**, 1305 (2023).
5. T. J. Foutz, M. Wong, Brain stimulation treatments in epilepsy: Basic mechanisms and clinical advances. *Biomed. J.* **45**, 27–37 (2022).
6. J. D. Rolston, S. A. Desai, N. G. Laxpati, R. E. Gross, Electrical stimulation for epilepsy: experimental approaches. *Neurosurgery Clinics of North America* **22**, 425–442 (2011).
7. R. S. Fisher, Neurostimulation for epilepsy: Do we know the best stimulation parameters? *Epilepsy Currents* **11**, 203–204 (2011).
8. S. Wong, R. Mani, S. Danish, Comparison and selection of current implantable anti-epileptic devices. *Neurotherapeutics* **16**, 369–380 (2019).
9. P. Ryvlin, S. Rheims, L. J. Hirsch, A. Sokolov, L. Jehi, Neuromodulation in epilepsy: state-of-the-art approved therapies. *The Lancet Neurology* **20**, 1038–1047 (2021).
10. T. G. Thomas, B. Jobst, Critical review of the responsive neurostimulator system for epilepsy. *Med. Devices (Auckl.)* **8**, 405–411 (2015).
11. R. Wang, P. E. McGoldrick, G. Subah, C. R. Muh, S. M. Wolf, Sudden unexpected death in epilepsy in a patient with a brain-responsive neurostimulation device. *Ann. Child Neurol. Soc.* **2**, 162–167 (2024).
12. Dallmer-Zerbe I, Jiruska P, Hlinka J. Personalized dynamic network models of the human brain as a future tool for planning and optimizing epilepsy therapy. *Epilepsia*. 2023; 64(9): 2221-2238.
13. G. Costa, C. Teixeira, M. F. Pinto, Comparison between epileptic seizure prediction and forecasting based on machine learning. *Scientific Reports* **14**, 5653 (2024).

14. S. Chiang, A. N. Khambhati, E. T. Wang, M. Vannucci, E. F. Chang, V. R. Rao, Evidence of state-dependence in the effectiveness of responsive neurostimulation for seizure modulation. *Brain Stimul.* **14**, 366–375 (2021).
15. D. N. Anderson, C. M. Charlebois, E. H. Smith, T. S. Davis, A. Y. Peters, B. J. Newman, A. M. Arain, K. S. Wilcox, C. R. Butson, J. D. Rolston, Closed-loop stimulation in periods with less epileptiform activity drives improved epilepsy outcomes. *Brain* **147**, 521–531 (2024).
16. C. Kaspar, B. J. Ravoo, W. G. van der Wiel, S. V. Wegner, W. H. P. Pernice, The rise of intelligent matter. *Nature* **594**, 345–355 (2021).
17. K. Roy, A. Jaiswal, P. Panda, Towards spike-based machine intelligence with neuromorphic computing. *Nature* **575**, 607–617 (2019).
18. A. Basu, L. Deng, C. Frenkel, X. Zhang, Spiking neural network integrated circuits: A review of trends and future directions. *2022 IEEE Custom Integrated Circuits Conference (CICC)*, 1–8 (2022).
19. J. W. Ephraim, D. Caron, Á. Canal-Alonso, J. M. Corchado, G. Palazzolo, G. Panuccio, Developing hippocampal spheroids model ictogenesis and epileptogenesis. *bioRxiv* (2023).
20. N. Fremaux, W. Gerstner, Neuromodulated spike-timing-dependent plasticity and theory of three-factor learning rules. *Front. Neural Circuits* **9**, 155830 (2016).
21. B. Petro, N. Kasabov, R. M. Kiss, Selection and optimization of temporal spike encoding methods for spiking neural networks. *IEEE Trans. Neural Netw. Learn. Syst.* **31**, 358–370 (2020).
22. R. J. Piper, R. M. Richardson, G. Worrell, D. W. Carmichael, T. Baldeweg, B. Litt, T. Denison, M. Tisdall, Towards network-guided neuromodulation for epilepsy. *Brain* **145**, 3347–3362 (2022).
23. Wu, Y.C.; Liao, Y.S.; Yeh, W.H.; Liang, S.F.; Shaw, F.Z. Directions of Deep Brain Stimulation for Epilepsy and Parkinson’s Disease. *Front. Neurosci.* **15**, 680938 (2021).
24. J. L. Alcalá-Zermeno, K. Starnes, N. M. Gregg, G. Worrell, B. N. Lundstrom, Responsive neurostimulation with low-frequency stimulation. *Epilepsia* **64**, e16–e22 (2023).
25. E. Paschen, P. Kleis, D.M. Vieira, K. Heining, C. Boehler, U. Egert, U. Häussler, C.A. Haas, On-demand low-frequency stimulation for seizure control: efficacy and behavioural implications, *Brain*, **147**, 2, 505–520, (2024).

26. S.-N. Lim, C.-Y. Lee, S.-T. Lee, P.-H. Tu, B.-L. Chang, C.-H. Lee, M.-Y. Cheng, C.-W. Chang, W.-E. J. Tseng, H.-Y. Hsieh, H.-I. Chiang, T. Wu, Low and high frequency hippocampal stimulation for drug-resistant mesial temporal lobe epilepsy. *Neuromodulation* **19**, 365–372 (2016).
27. S. Carrette, P. Boon, M. Sprengers, R. Raedt, K. Vonck, Responsive neurostimulation in epilepsy. *Expert Rev. Neurother.* **15**, 1445–1454 (2015).
28. G. Panuccio, A. Guez, R. Vincent, M. Avoli, J. Pineau, Adaptive control of epileptiform excitability in an in vitro model of limbic seizures. *Exp. Neurol.* **241**, 179–183 (2013).
29. D. Caron, Á. Canal-Alonso, G. Panuccio, Mimicking CA3 temporal dynamics controls limbic ictogenesis. *Biology* **11**, 371 (2022).
30. J. Chvojka, J. Kudlacek, W.-C. Chang, O. Novak, F. Tomaska, J. Otahal, J. G. R. Jefferys, P. Jiruska, The role of interictal discharges in ictogenesis — A dynamical perspective. *Epilepsy Behav.* **121**, 106591 (2021).
31. G. Panuccio, I. Colombi, M. Chiappalone, Recording and modulation of epileptiform activity in rodent brain slices coupled to microelectrode arrays. *J. Vis. Exp.* (135), e57548 (2018).
32. S. Gollwitzer, R. Hopfengärtner, K. Rössler, T. Müller, D. G. Olmes, J. Lang, J. Köhn, M. D. Onugoren, J. Heyne, S. Schwab, H. M. Hamer, Afterdischarges elicited by cortical electric stimulation in humans: When do they occur and what do they mean? *Epilepsy Behav.* **87**, 173–179 (2018).
33. M. B. Westover, J. Cormier, M. T. Bianchi, M. Shafi, R. Kilbride, A. J. Cole, S. S. Cash, Revising the “Rule of Three” for inferring seizure freedom. *Epilepsia* **53**, 368–376 (2012).